

See discussions, stats, and author profiles for this publication at: <https://www.researchgate.net/publication/345369983>

# GrabRiver: Graph-Theory-Based River Width Extraction From Remote Sensing Imagery

Article in IEEE Geoscience and Remote Sensing Letters · September 2020

DOI: 10.1109/LGRS.2020.3023043

---

CITATIONS

0

READS

91

5 authors, including:



Yi Lin

Zhejiang University of Technology

16 PUBLICATIONS 122 CITATIONS

[SEE PROFILE](#)



Junguo Liu

Beijing Forestry University

257 PUBLICATIONS 7,906 CITATIONS

[SEE PROFILE](#)

Some of the authors of this publication are also working on these related projects:



Research on virtual water and water footprint [View project](#)



China ecosystem management and strategy, funded by CCICED [View project](#)

# GrabRiver: Graph-Theory-Based River Width Extraction From Remote Sensing Imagery

Zifeng Wang, *Member, IEEE*, Jinbao Li, Yi Lin, Ying Meng, and Junguo Liu<sup>ID</sup>

**Abstract**—River width can reveal the water extent and water flow on the earth’s surface. Remote sensing facilitates river width extraction at large scales in an automatic way. This letter proposes a new method named GrabRiver that implements whole-process automation from image preparation to river width calculation. It also, for the first time, develops river graph as the simultaneous river topology for width extraction, combining river planform morphology and network. Three major steps are proposed: 1) mapping and connecting rivers. The Multispectral Water Index (MuWI) is used to produce high-accuracy water maps from imagery, whereby specialized algorithms are used to reduce the impacts from nonriver water (lakes, reservoirs, wetlands) and on-channel objects (bridges, dams, ships) and to enforce river connectivity; 2) Constructing the river graph. A connected river map is skeletonized into the graph while maintaining georeferences as properties of edges and nodes in the river graph, and it is followed by river graph pruning to remove false and redundant river tributaries in the topologic structure; and 3) Measuring river widths. The cross-sectional measure is conducted on the river-reach (graph edge) basis, where orthogonals to centerlines are determined by the bounding geometry. In our experiments, the output results of GrabRiver are consistent with the reference river widths ( $R^2 = 0.98$  in the mean width validation and  $R^2 = 0.91$  in the transient width validation). Despite that GrabRiver is a promising method, random uncertainty in water mapping is identified as the major source of width measurement errors. The outputs of GrabRiver will be applicable in fluvial analysis and satellite-derived discharge estimates.

**Index Terms**—Fluvial geomorphology, Google Earth Engine (GEE), graph theory, river network, river width.

Manuscript received June 25, 2020; revised August 17, 2020; accepted September 6, 2020. This work was supported in part by the Strategic Priority Research Program of Chinese Academy of Sciences under Grant XDA20060402, in part by the National Natural Science Foundation of China (NSFC) under Grant 41625001, in part by the Pengcheng Scholar Program of Shenzhen, in part by the National High-Level Talents Special Support Plan (“Ten Thousand Talents Plan”), in part by the Leading Innovative Talent Program for Young and Middle-Aged Scholars by the Ministry of Science and Technology, and in part by the High-Level Special Funding of the Southern University of Science and Technology under Grant G02296302 and Grant G02296402. (*Corresponding author: Junguo Liu*.)

Zifeng Wang is with the School of Environmental Science and Engineering, Southern University of Science and Technology, Shenzhen 518055, China, and also with the Department of Geography, The University of Hong Kong, Hong Kong (e-mail: wzfeng@hku.hk).

Jinbao Li and Yi Lin are with the Department of Geography, The University of Hong Kong, Hong Kong.

Ying Meng and Junguo Liu are with the School of Environmental Science and Engineering, Southern University of Science and Technology, Shenzhen 518055, China (e-mail: junguo.liu@gmail.com).

Color versions of one or more of the figures in this letter are available online at <http://ieeexplore.ieee.org>.

Digital Object Identifier 10.1109/LGRS.2020.3023043

## I. INTRODUCTION

IN RESOLVING the notable problem of the Seven Bridges of Königsberg, Leonhard Euler established the basis of graph theory, a foundation of discrete mathematics and computer science [1]. A revisit of the original problem inspired the possibility of extracting river morphology based on graph because Euler’s answer builds the land graph while different land parts are divided by the river system (see Fig. 1).

River width is of high interest among many quantities of river planform morphology because it is one of the two fundamental dimensions of river extent (i.e., width and length) and is one of the principal components of river discharge (i.e., width, depth, and velocity). Therefore, river width is associated with many hydrological, hydraulic, and biogeochemical processes through river extent, river discharge, or both, such as floods, ice freeze, sediment transport, and carbon dioxide emissions [2]–[4]. Specifically, recent advances in satellite-derived river discharge highlight the importance of river width measurements [5]–[7].

Graph can be an effective tool for representing complex river networks (e.g., braided river) [8] and for modeling reach-level river morphology, as the edge in a graph can naturally correspond to the river reach in the physical world. Extracting river width in accordance with river graph can not only preserve the respective utilities of river width measurement and river graph representation but also expect collective advantages, such as enhanced river routing.

Several methods have been proposed for river width extraction by remote sensing [9]–[11]. However, these methods have tended to associate the measurements with many cross sections rather than the river system as a whole, which leads to incomplete topology and thus hinders the possible broader applicability of river width information. Furthermore, the on-channel constructions (e.g., dams, bridges, and ships) can impede the extraction of river connectivity, which is not explicitly considered in the existing methods of river width extraction [9]–[11] or even river network extraction [8], [12].

In this regard, this letter aims to present a graph-theory-based river width extraction from remote sensing imagery (GrabRiver), a new method and tool that enables simultaneous extractions of river topology and river width based on graph theory and maintains the integrity of river connectivity. The GrabRiver method links with the Google Earth Engine (GEE) platform [13] for seamless automation of procedures, from imagery acquisition and preprocessing (e.g., cloud-removal) to the final extractions of river width.

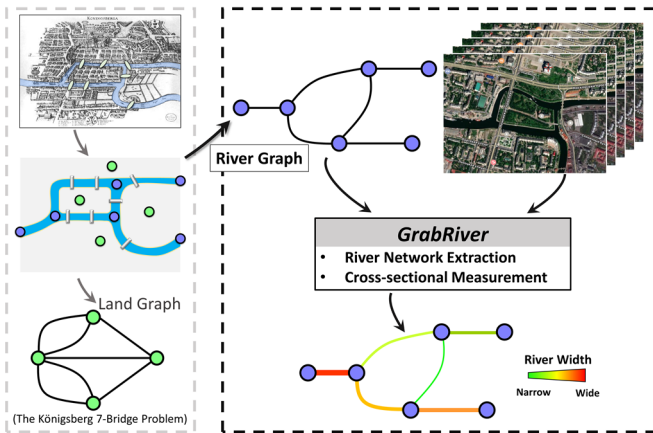


Fig. 1. Schematic flowchart of the proposed graph-theory-based river width extraction inspired by the classic problem.

## II. METHODOLOGY

In general, the algorithm used in GrabRiver includes three major steps: 1) mapping and connecting rivers; 2) constructing river graph; and 3) measuring river widths. Detailed procedures are shown in Fig. 2, and the associated approaches will be described in this section. We adopted Sentinel-2 imagery to implement and validate GrabRiver due to its high spatial and spectral resolutions.

### A. Mapping and Connecting Rivers

Water pixels are first identified from multispectral imagery. To avoid cloud contaminations, scene-wise and pixel-wise quality controls are applied in the image selection. Only scenes with less than 10% cloud cover percentage are selected, while both opaque and cirrus cloud pixels are excluded using the QA60 band of Sentinel-2 [14] as the mask. Water pixels are then identified through the calculation of the Multi-spectral Water Index (MuWI) [15] as in (1), which can deliver the native 10-m water response map based on the Sentinel-2 bands of multiple resolutions (10-m, 20-m, 60-m) [see Fig. 2(b)].

$$\begin{aligned} \text{MuWI} &= -4\text{ND}_{2,3} + 2\text{ND}_{3,8} + 2\text{ND}_{3,12} - \text{ND}_{3,11} \\ &= -4 \times \frac{\rho_{\text{blue}} - \rho_{\text{green}}}{\rho_{\text{blue}} + \rho_{\text{green}}} + 2 \times \frac{\rho_{\text{green}} - \rho_{\text{NIR}}}{\rho_{\text{green}} + \rho_{\text{NIR}}} \\ &\quad + 2 \times \frac{\rho_{\text{green}} - \rho_{\text{SWIR2}}}{\rho_{\text{green}} + \rho_{\text{SWIR2}}} - \frac{\rho_{\text{green}} - \rho_{\text{SWIR1}}}{\rho_{\text{green}} + \rho_{\text{SWIR1}}} \end{aligned} \quad (1)$$

where  $\text{ND}_{i,j}$  denotes the normalized difference of two bands where subscripts  $i, j$  represent the band numbers on Sentinel-2;  $\rho$  denotes the reflectance value where the subscript represents the band name. Compared with previous water indexes, MuWI can effectively improve the low-albedo identification that is often confused with shadows (from terrain, built-up, and cloud) and asphalt roads [15], [16].

After calculating the MuWI, the histogram-based Otsu's algorithm is used to automatically determine the MuWI threshold for classifying water and nonwater pixels. As shown in Fig. 2(c), the determined binary water map contains nonriver water pixels, such as wetlands, lakes and reservoirs, and independent channels that are not connected to the river system. The GrabRiver filters out those nonriver water pixels by

detecting the connected components in the water map and then applying the size filter. A default  $\sim 2.0 \text{ km}^2$  (20 000 Sentinel-2 pixels) is set as the threshold for the size filter and can be customized in the tool, which means a single connected water body smaller than  $\sim 2.0 \text{ km}^2$  will be excluded.

The filtered channel map [see Fig. 2(d)] is converted to the river map [see Fig. 2(e)] by removing the small islands because the islands of relatively small areas contribute to the unnecessarily excessive topological complexity and computations in the extraction [9], [10]. Islands with areas smaller than  $\sim 0.6 \text{ km}^2$  (6000 pixels) are removed and the threshold can be customized for other applications.

To enforce the connectivity in the river map, morphological transformations are applied to connect river pixels impacted by the on-channel objects, such as dams, bridges, and ships. The closing operation is first performed with a  $5 \times 5$  size kernel, which aims to fill in gaps inside the water body. A dilation followed by thinning is subsequently applied to connect the adjacent water bodies that are partly or entirely broken by the on-channel objects [see Fig. 2(e) and (f)]. GrabRiver implements the image selection and MuWI calculation through GEE air position indicator (API) [13], and thus the input image can be acquired directly from the data catalog on the cloud platform.

### B. Constructing River Graph

The graph is built upon the one-pixel wide river centerlines with connectivity maintained. A specialized algorithm of connectivity enforcing has been devised for the river map, so that the connected river centerlines can be directly extracted. The centerlines are extracted using the skeletonization (or thinning) algorithm [17] [see Fig. 2(h)]. A prerequisite processing—distance transform—is illustrated in Fig. 2(g) that computes the distance of the river pixel to the nearest nonriver pixel. The binary pixel-wise topology in the river centerlines is then transformed into the network topology in the form of graph [see Fig. 2(i)]. The node in the river graph represents the river confluence, while the edge in the river graph represents the river reach without any tributary. The multigraph, which permits multiple edges between two nodes (parallel edges), is used to adapt to the rejoined braided river channels, as shown in the example case. The constructed river graph stores the geographic coordinates corresponding to the nodes and edges as their properties, so that the river graph can be easily mapped to the geographic spaces. Meanwhile, the length of the edge (river reach) can be calculated (as the edge weight) based on those geographic coordinates for further network or graph analysis.

However, as the skeletonization algorithm is designed for general image processing rather than river-specialized purposes, false or unfavorable tributaries may be generated. Such flaw propagates to the construction of river graph, resulting in unrealistic river representation with too many nodes and edges. To address the issue, the initial river graph is pruned to remove false tributaries. River graph pruning is performed according to 1) the degree of the nodes and 2) the length of the edges. If any degree of the two nodes on an edge equals 1 and the edge is a short tributary, this edge and the end

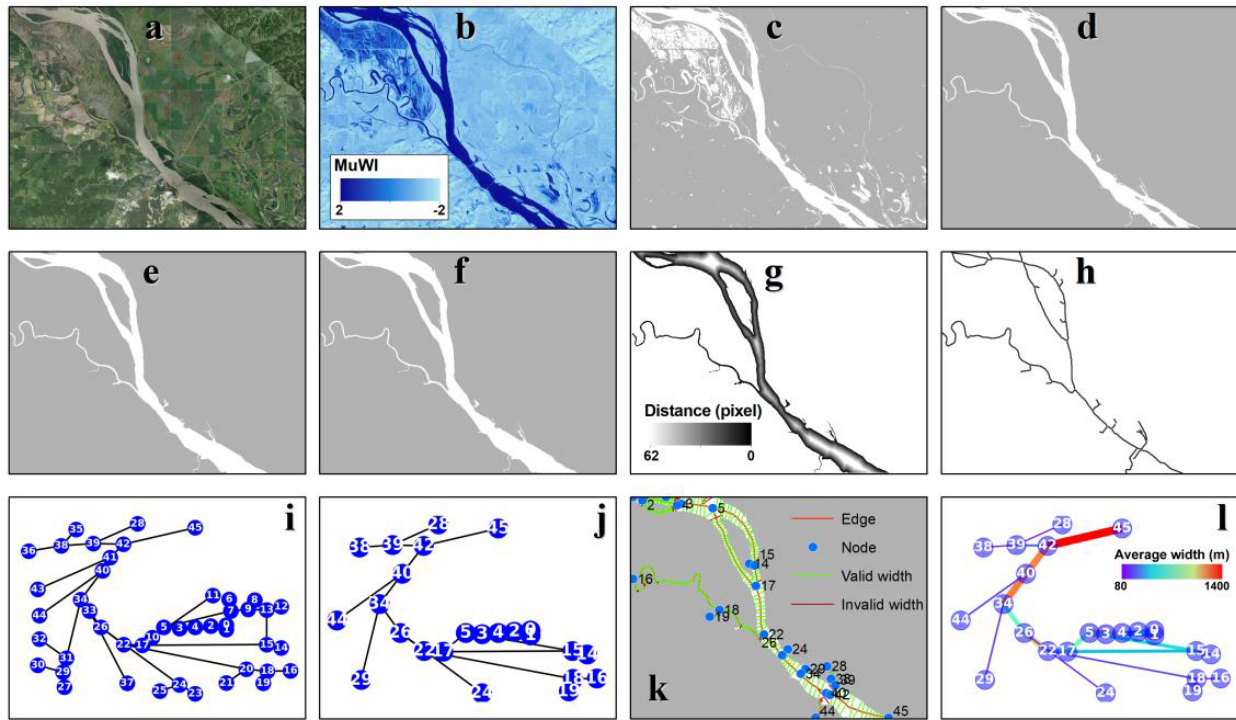


Fig. 2. Detailed steps to extract river width from remote sensing imagery. (a) Satellite imagery. (b) MuWI water probability map. (c) Binary water map. (d) Channel map. (e) River map. (f) River map with enforced connectivity. (g) Map of the distance to the nearest land. (h) Initial river centerlines. (i) Initial river graph. (j) Pruned river graph. (k) Pruned river graph mapped back to geographic space with cross sections. (l) River graph with width measurements.

node ( $\text{degree} = 1$ ) will be removed from the graph. A short tributary is identified by either of the following two criteria: 1) the length of the edge is less than a user-defined threshold (default = 50 pixels) and 2) the relative length of the edge to the maximum river distance (to land) on the edge is less than 2.5. The absolute length criterion can eliminate the ends of small-order streams in the graph. The relative length criterion can remove false tributaries in a wide river channel. After pruning the edges and their associated end nodes, the degree of each node in the river graph is recalculated. Some newly formed middle nodes ( $\text{degree} = 2$ ) are subsequently removed, and their two neighboring nodes are connected directly. River graph pruning can be performed by iterations until satisfactory simplification. Fig. 2(j) shows the pruned river graph after one iteration where the number of nodes decreased from 46 to 24 and the number of edges decreased from 47 to 25. The pruned river graph is mapped back to the geographic space as in Fig. 2(k).

### C. Measuring River Widths

River widths are measured at cross sections that are set in accordance with the edges (river reaches) in the river graph. For each edge, it first acts as the river centerlines to generate the cross sections that are orthogonal to their local river centerline direction. To identify the orthogonal angle, bounding geometry instead of two end pixels is used (see Fig. 3). When identifying the orthogonal angle of a centerline pixel, a number of forward-adjacent and backward-adjacent centerline pixels are selected (by default, four forward and four backward pixels). The algorithm calculates a possibly

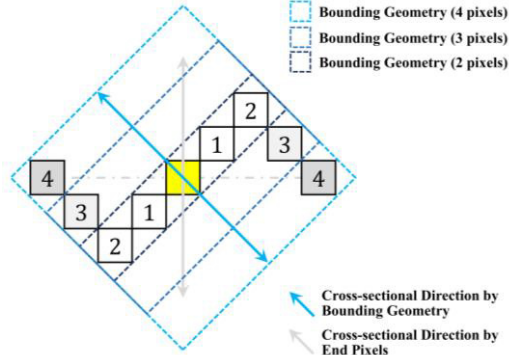


Fig. 3. Schematic determination of the orthogonal angle to the centerline pixels by the bounding geometry.

rotated rectangle of the minimum area that encloses all the selected pixels, that is, the bounding geometry. The orthogonal angle of a centerline pixel is proximate to the width side angle of the bounding geometry. Compared with the orthogonal identification approach based on only two end pixels, the bounding geometry approach can be more robust to extreme cases, such as the S-shaped centerline. The orthogonal change between the adjacent centerline pixels can be smoother as more pixels are taken into account for angle calculation.

After orthogonal angle identification, the orthogonal line (cross section) extends from the centerline pixel to the two river banks. The initial cross section is as long as 3.6 times the distance to land at the centerline pixel location. The river width measurement, thus, becomes the shortening of the initial cross section. The initial cross section keeps shortened by 1 pixel at

a time until both ends touch the water extent identified in the previous step. The Euclidean distance between the two end pixels on the cross section under a projection is assigned as the river width at the centerline location.

The sampling density of the cross sections, as well as of the river widths, can be modified in the tool to reduce computations. For example, the sampling interval in Fig. 2(k) is proportional to the distance to land at the centerline location. Invalid width measurements are finally detected based on whether or not any end of the cross section is within the water rather than on the water–bank interface. Such invalid width measurements are often located near the node (confluence). Since the measurement is performed per edge, the widths and the cross sections can be stored in the edge, contributing as quantities of the river graph [see Fig. 2(l)].

### III. RESULTS AND DISCUSSION

To demonstrate the efficiency and accuracy of GrabRiver, we implement and validate the river width measurements over the Mekong River and Mississippi River. The Mekong River case (sample size  $n = 77$ ) is used to test the mean river width measurement compared with the manually measured values on the high-resolution Bing Aerial imagery. The Mississippi River case (sample size  $n = 114$ ) is used to test the same-day river width measurements compared with the *in situ* measurements by the United States Geological Survey (USGS). The mean river width is more commonly used in spatial pattern analysis, such as river extent mapping. The same-day width intends to capture the transient status of a river and is often used for tasks sensitive to temporal variations, such as discharge derivation. GrabRiver successfully produces width measurements of satisfactory accuracies in the two general uses.

Fig. 4(a) presents the mean width measurements in the Mekong River basin. The composite Sentinel-2 images with 50% percentile [16] are used as the input data. The mean river widths derived from Sentinel-2 are highly consistent with the reference widths from high-resolution imagery ( $R^2 = 0.98$ , mean bias =  $-17.16$  m, mean absolute error =  $26.05$  m, and root-mean-square error =  $47.3$  m). As the reference width finds its derived counterpart by joining the closest cross section rather than cross section with the exact same coordinates, the location discrepancy can contribute to the mismatch between the derived and reference mean widths. A closer examination of the suspicious outlier (the rightmost point) identifies its location in the estuary where parallel channels are common and close to the measured river channel due to low relief. The large error at this point is because one end of the cross section is falsely calculated in the near parallel channel rather than in the measured channel. Although this kind of impact from the parallel channel is uncommon in most basin areas, it can suggest a smaller length of initial cross section (3.6 times of distance to land in this case) or an alternative width-measuring approach starting from the centerline (current approach starts from the ends).

Fig. 4(b) shows the same-day measurements in the Mississippi River basin. The Sentinel-2-derived river widths are in general agreement with the *in situ* measurements ( $R^2 = 0.91$ , mean bias =  $-5.81$ , mean absolute error =  $36.67$ , and root-

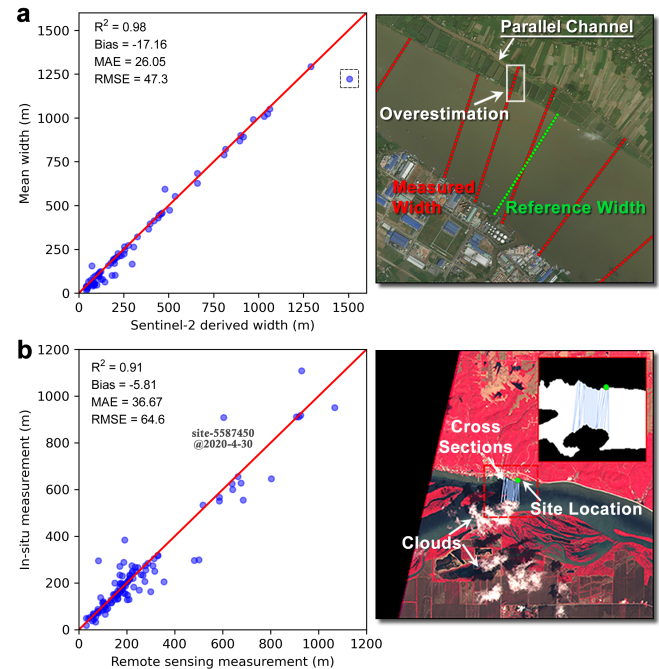


Fig. 4. Validation of (a) mean width extractions in the Mekong River basin with a map of parallel channel issue and (b) transient width extractions in the Mississippi River basin with a map of cirrus cloud.

mean-square error =  $64.6$ ). Despite the overall high accuracy, the same-day measurements on individual images yield relatively high error variance, particularly against the mean measurements (see Fig. 4). Broadly speaking, the random uncertainties in individual images may lead to unexpected water mapping, which could be the main reason for the high error variance. In contrast, those random uncertainties can be minimized in the composite image because the percentile calculation on a stack of images can largely exclude extremes [15], [18]. One of the major sources of random uncertainties is the cloud. For example, on the image over site 5587450 (USGS gauge ID) on May 30, 2020 [annotated in Fig. 4(b)], a thin, semitransparent cirrus cloud happens to be located close to the site on the river channel, which contributes to water mapping omissions and thus an underestimated river width. Although scene- and pixel-wise cloud removals have been applied (Section II-A), the state-of-the-art cloud removal algorithm cannot guarantee each pixel, particularly in the challenging case of thin cirrus cloud over water [19]. Meanwhile, it is also observed that snow and ice can induce the false detection of water bodies, especially from images over the upper Mississippi. Finally, random uncertainty could also be caused by the local land:water ratio, as the adopted Otsu's thresholding method used to classify water and nonwater pixels is sensitive to the skewness of the MuWI histogram where the left-skewed histogram (high land percentage) can underestimate the threshold [20] and overestimate the water extent, and vice versa. Therefore, we further constrain Otsu's thresholding within the range  $[0, 0.9]$ .

Table I summarizes the accuracy assessment of GrabRiver and RivWidth in the case of mean width extraction. Both the methods deliver similarly high accuracies for all rivers, while GrabRiver presents marginally better performance

TABLE I  
SUMMARY OF RIVER WIDTH EXTRACTION ACCURACY

Metrics	GrabRiver	RivWidth <sup>a</sup>
<u>All River Sizes</u>		
R <sup>2</sup>	0.98	0.98
Bias	-17.16	7.96
MAE	26.05	30.85
RMSE	47.3	46.4
<u>Small to Middle Rivers</u>		
R <sup>2</sup>	0.93	0.87
Bias	-17.21	3.47
MAE	22.12	29.3
RMSE	34.3	47.1

<sup>a</sup>RivWidth results are extracted from [23].

for small to middle rivers perhaps because it uses 10-m Sentinel-2 imagery.

As shown in both the cases, water mapping could be the primary source of the measurement error in river width. For more accurate river width extraction, improved water mapping could be made by more sophisticated thresholding, for example, by integrating global and local thresholding, and assessing other thresholding methods (such as adaptive methods [21]), using prior information (such as predefined water location data [22], [23]). Recent progress in deep learning may also augment water mapping, particularly in extreme situations [24]. However, some inherent issues from optical imagery can undermine water mapping, of which the most prominent is perhaps cloud impact [25]. A possible future improvement is to fuse synthetic aperture radar (SAR) images for river detection, as it can penetrate the clouds so that the river width extraction would be less affected by weather conditions.

Our proposed method is not resolution-dependent, but the current demonstration on Sentinel-2 with 10-m resolution could be most useful for stream order 3 or larger rivers. Despite that we demonstrate GrabRiver on Sentinel-2 imagery, other remote sensing imagery, such as Landsat and Moderate Resolution Imaging Spectroradiometer (MODIS), can be used as the data source. For imagery without all the reflectance required in (1) (e.g., 4-band aerial imagery), GrabRiver can be a potential tool only if a MuWI-like water probability map is calculated.

#### IV. CONCLUSION

In this letter, we proposed GrabRiver for river width extraction from remote sensing imagery. The proposed method is the first of its kind to extract river width based on the river graph that is simultaneously derived. It combines the strengths of graph theory with novel approaches of water mapping and cross-sectional width measurement. The proposed method is capable of accurately and effectively extracting river widths based on Sentinel-2 images, in the scenarios of both mean width extraction and transient width extraction. The integrative design not only facilitates high accuracy river width extraction through a high level of process automation from image preparation to the final calculation but also allows further investigation of river system variations in the Anthropocene.

#### REFERENCES

- [1] N. Biggs, E. K. Lloyd, and R. J. Wilson, *Graph Theory*. Oxford, U.K.: Clarendon, 1986, pp. 1736–1936.
- [2] J. P. Benstead and D. S. Leigh, “An expanded role for river networks,” *Nature Geosci.*, vol. 5, no. 10, pp. 678–679, Oct. 2012.
- [3] X. Yang, T. M. Pavelsky, and G. H. Allen, “The past and future of global river ice,” *Nature*, vol. 577, no. 7788, pp. 69–73, Jan. 2020.
- [4] P. Lin *et al.*, “Global estimates of reach-level bankfull river width leveraging big data geospatial analysis,” *Geophys. Res. Lett.*, vol. 47, no. 7, Apr. 2020, Art. no. e2019GL086405.
- [5] D. E. Alsdorf, E. Rodríguez, and D. P. Lettenmaier, “Measuring surface water from space,” *Rev. Geophys.*, vol. 45, no. 2, May 2007, Art. no. RG2002.
- [6] D. Yamazaki, F. O’Loughlin, M. A. Trigg, Z. F. Miller, T. M. Pavelsky, and P. D. Bates, “Development of the global width database for large rivers,” *Water Resour. Res.*, vol. 50, no. 4, pp. 3467–3480, Apr. 2014.
- [7] C. J. Gleason and L. C. Smith, “Toward global mapping of river discharge using satellite images and at-many-stations hydraulic geometry,” *Proc. Nat. Acad. Sci. USA*, vol. 111, no. 13, pp. 4788–4791, Apr. 2014.
- [8] G. Connor-Streich, A. J. Henshaw, J. Brasington, W. Bertoldi, and G. L. Harvey, “Let’s get connected: A new graph theory-based approach and toolbox for understanding braided river morphodynamics,” *Wiley Interdiscipl. Rev. Water*, vol. 5, no. 5, p. e1296, Sep. 2018.
- [9] X. Yang, T. M. Pavelsky, G. H. Allen, and G. Donchyts, “RivWidth-Cloud: An automated Google Earth engine algorithm for river width extraction from remotely sensed imagery,” *IEEE Geosci. Remote Sens. Lett.*, vol. 17, no. 2, pp. 217–221, Feb. 2020.
- [10] T. M. Pavelsky and L. C. Smith, “RivWidth: A software tool for the calculation of river widths from remotely sensed imagery,” *IEEE Geosci. Remote Sens. Lett.*, vol. 5, no. 1, pp. 70–73, Jan. 2008.
- [11] F. Isikdogan, A. Bovik, and P. Passalacqua, “RivaMap: An automated river analysis and mapping engine,” *Remote Sens. Environ.*, vol. 202, pp. 88–97, Dec. 2017.
- [12] X. Chen *et al.*, “Construct channel network topology from remote sensing images by morphology and graph analysis,” *IEEE Geosci. Remote Sens. Lett.*, vol. 17, no. 7, pp. 1163–1167, Jul. 2020.
- [13] N. Gorelick, M. Hancher, M. Dixon, S. Ilyushchenko, D. Thau, and R. Moore, “Google Earth engine: Planetary-scale geospatial analysis for everyone,” *Remote Sens. Environ.*, vol. 202, pp. 18–27, Dec. 2017.
- [14] M. Drusch *et al.*, “Sentinel-2: ESA’s optical high-resolution mission for GMES operational services,” *Remote Sens. Environ.*, vol. 120, pp. 25–36, May 2012.
- [15] Z. Wang, J. Liu, J. Li, and D. Zhang, “Multi-spectral water index (MuWI): A native 10-m multi-spectral water index for accurate water mapping on Sentinel-2,” *Remote Sens.*, vol. 10, no. 10, p. 1643, Oct. 2018.
- [16] Y. Lin, Z. Wang, C. Y. Jim, J. Li, J. Deng, and J. Liu, “Water as an urban heat sink: Blue infrastructure alleviates urban heat island effect in mega-city agglomeration,” *J. Cleaner Prod.*, vol. 262, Jul. 2020, Art. no. 121411.
- [17] T. Y. Zhang and C. Y. Suen, “A fast parallel algorithm for thinning digital patterns,” *Commun. ACM*, vol. 27, no. 3, pp. 236–239, Mar. 1984.
- [18] A. C. Ortiz, S. Roy, and D. A. Edmonds, “Land loss by pond expansion on the Mississippi river delta plain,” *Geophys. Res. Lett.*, vol. 44, no. 8, pp. 3635–3642, Apr. 2017.
- [19] Z. Zhu, S. Wang, and C. E. Woodcock, “Improvement and expansion of the FMASK algorithm: Cloud, cloud shadow, and snow detection for Landsats 4–7, 8, and Sentinel 2 images,” *Remote Sens. Environ.*, vol. 159, pp. 269–277, Mar. 2015.
- [20] G. Donchyts, J. Schellekens, H. Winsemius, E. Eisemann, and N. van de Giesen, “A 30 m resolution surface water mask including estimation of positional and thematic differences using Landsat 8, SRTM and OpenStreetMap: A case study in the Murray-Darling basin, Australia,” *Remote Sens.*, vol. 8, no. 5, p. 386, May 2016.
- [21] J. Bobin, J.-L. Starck, J. M. Fadili, Y. Moudden, and D. L. Donoho, “Morphological component analysis: An adaptive thresholding strategy,” *IEEE Trans. Image Process.*, vol. 16, no. 11, pp. 2675–2681, Nov. 2007.
- [22] G. H. Allen and T. M. Pavelsky, “Patterns of river width and surface area revealed by the satellite-derived North American river width data set,” *Geophys. Res. Lett.*, vol. 42, no. 2, pp. 395–402, Jan. 2015.
- [23] G. H. Allen and T. M. Pavelsky, “Global extent of rivers and streams,” *Science*, vol. 361, no. 6402, pp. 585–588, Aug. 2018.
- [24] L. F. Isikdogan, A. Bovik, and P. Passalacqua, “Seeing through the clouds with deepwatermap,” *IEEE Geosci. Remote Sens. Lett.*, early access, Nov. 26, 2019, doi: 10.1109/LGRS.2019.2953261.
- [25] C. Huang, Y. Chen, S. Zhang, and J. Wu, “Detecting, extracting, and monitoring surface water from space using optical sensors: A review,” *Rev. Geophys.*, vol. 56, no. 2, pp. 333–360, Jun. 2018.